Hybrid Controller Concept for Dynamic Positioning of Marine Vessels with Experimental Results ⋆

Astrid H. Brodtkorb [a] Svenn A. Værnø [a] Andrew R. Teel [b] Asgeir J. Sørensen [a] Roger Skjetne [a]

[a] *Centre for Autonomous Marine Operations and Systems, Department of Marine Technology, Norwegian University of Science and Technology (NTNU AMOS), 7491 Trondheim, Norway (e-mails: astrid.h.brodtkorb@ntnu.no, svenn.are.varno@ntnu.no, asgeir.sorensen@ntnu.no, roger.skjetne@ntnu.no).*

[b] *Department of Electrical and Computational Engineering, University of California Santa Barbara, CA 93106-9560 USA (e-mail: teel@ece.ucsb.edu)*

Abstract

The next generation marine control systems will, as a step towards increased autonomy, have more automatic functionality in order to cope with a set of complex operations in unknown, challenging and varying environments while maintaining safety and keeping operational costs low. In this paper a hybrid control strategy for stationkeeping and maneuvering of marine vessels is proposed. The hybrid concept allows a structured way to develop a control system with a bank of controllers and observers improving dynamic positioning (DP) performance in stationary dynamics, changing dynamics including enhancing transient performance, and giving robustness to measurement errors. DP systems are used on marine vessels for automatic stationkeeping and tracking operations solely by use of the thrusters. In this paper a novel method improving the transient response of a vessel in DP is developed. The performance of the hybrid control system, including two observer candidates and one controller candidate, is demonstrated in model-scale experiments and on full-scale field data. The hybrid system has global stability properties.

Key words: Marine control systems, hybrid systems, dynamic positioning, observers, output feedback control

1 Introduction

Marine operations are moving into harsher environments, and as a consequence, requirements for the vessel's operational window, safety functions, and energy-efficiency become stricter (Sørensen, 2011). As a result, the level of autonomy in marine control systems is increasing, with automatic performance monitoring and switching. During marine operations, both variations in stationary dynamics and transient behavior are important to account for in an all-year operation philosophy subject to changing weather, sea loads, and modes of operation (Perez, Sørensen, and Blanke, 2006). There are many unknown factors that may cause transients in the vessel response, both from the environment (e.g., wave trains and wind gusts) and triggered by the operation taking place (e.g., heading changes or crane operations of heavy goods). Figure 1 shows a marine vessel with its operational conditions and a block diagram of a general hybrid marine control system. The vessel operational conditions with *use mode, speed*, and *environment* indicates how the vessel performs different tasks with varying speed in an unknown and changing environment. The use mode includes algorithms that satisfy different control objectives such as stationkeeping, maneuvering, and target tracking, which is closely linked with the vessel speed. Environment refers to the state of the environment consisting of wind, waves and current. Naturally, certain operations can only be performed in calm conditions. Because different physical effects matter for the various vessel operational conditions, there are distinct models and control strategies which are designed specifically for each operational condition. Nguyen, Sørensen, and Quek (2007) proposed to use supervisory switched control based on the methodology of Hespanha and Morse (2002); Hespanha, Liber-

⋆ This work was supported by the Research Council of Norway through the Centres of Excellence funding scheme, project number 223254 - NTNU AMOS, and in part by NSF grant number ECCS-1508757 and AFOSR grant number FA9550-15-1-0155.

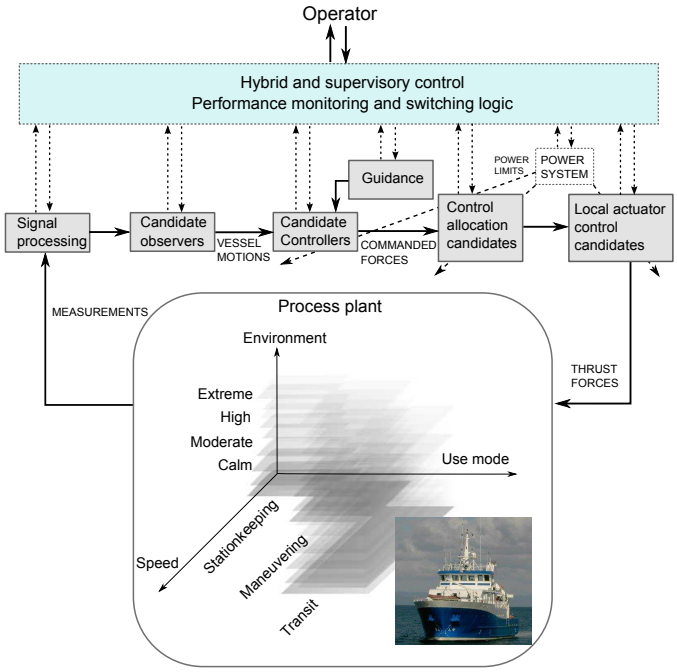

Fig. 1. Block diagram of a hybrid control system for a marine vessel in an unknown environment consisting of wind, waves and current. Sensors measure the operational status and vessel motions, and signal processing software filters, weights and votes between redundant measurements. The performance monitoring monitors the performance of the different blocks, and the switching logic chooses which algorithms to use in closed-loop control from the candidates. Here two observers and one controller are used.

zon, and Morse (2003). In addition to handling different speed regimes, use modes and changing sea states, the proposed setup ensures redundancy in the (software) *design methodology* so that faults (Blanke, Kinnaert, Lunze, and Staroswiecki, 2003) may be detected early and alarms may be raised to operators, who are either on-site or remote. The performance monitoring and switching logic block includes monitoring of the environment, power system, observer performance, position precision, signal health, and more. In order to ensure safety, there are high requirements for system reconfiguration, fault tolerance and redundancy, and for testing and verification of performance (DNV-GL, 2014). Testing and verification of marine control systems with higher levels of autonomy are faced with a large (when not infinite) number of failiure modes (Smogeli, Vik, Haugen, and Pivano, 2014); exhaustive testing is rarely possible. Therefore having modular design and proofs of subsystem properties may play a larger role in assuring safety (Kapinski, Deshmukh, Jin, Ito, and Butts, 2016). Systems with a wide range of dynamics and different modes that also use hybrid control approaches are for instance air traffic control (Sastry, Meyer, Tomlin, Lygeros, Godbole, and Pappas, 1995; Hu, Prandini, and Sastry, 2005), adaptive cruise control for the automotive industry (Girard, Howell, and Hedrick, 2005), autonomous docking operations of spacecraft (Malladi, Sanfelice, Butcher, and Wang, 2016), and in the marine industry hybrid power plants (Miyazaki, Sørensen, and Vartdal, 2016). The focus of this paper is on detecting and improving the transient performance of the DP control system using the hybrid system framework as proposed in Goebel, Sanfelice, and Teel (2012). As shown in Figure 1, it is believed that the concept of hybrid control can provide a scalable and stringent methodology for the design of real industrial control applications dealing with several control objectives and changing environmental and operational conditions. A similar, or alternative, method may be to consider robust control by multiple model adaptive controllers as proposed by Hassani, Sørensen, Pascoal, and Dong (2012); Hassani, Sørensen, Pascoal, and Athans (2017).

The main scientific contribution of this paper is the development of a hybrid control concept for proper switching of candidate observers and controllers, customized for transient and steady-state behavior of DP vessels. For particular observer candidates, this work combines a model-based observer (Fossen and Strand, 1999), a signal-based observer (Grip, Fossen, Johansen, and Saberi, 2015), a controller, and switching logic into a hybrid system with the goal of improving the transient response. The model-based observer, including wave filtering and bias force estimation, is especially suited in steady state, while the signal-based observer is more reactive during transients, even though it is more sensitive to signal noise. Stability analysis of the hybrid system applies results from Goebel, Sanfelice, and Teel (2009). Performance of the proposed concept is demonstrated experimentally through model-scale experiments with the hybrid observer estimates used in closed-loop output feedback control, and through estimation on full-scale field data. The paper is a continuation of Brodtkorb, Værnø, Teel, Sørensen, and Skjetne (2016), with the signal-based observer exchanged with one that has global stability properties, enhanced performance monitoring and switching logic, and new hybrid stability analysis.

The paper is organized as follows: The measurements and notation is introduced in Section 2, and the candidate observers and control algorithms are presented in Section 3. The hybrid system is assembled in Section 4, and stability is discussed in Section 5. The experimental setup and results are shown in Section 6. Section 7 concludes the paper.

2 Preliminaries

Common instrumentation in DP vessels includes position reference systems (typically GNSS [1]), compass, and inertial measurement units (IMU). The measurements,

[1] Global Navigation Satellite System

denoted with subscript m, are in this paper assumed to be of the form

$$p_m^n = [N, E]^\top \tag{1a}$$
$$\psi_m^n = \psi \tag{1b}$$
$$\omega_m^b = \omega^b + b_g \tag{1c}$$
$$f_m^b = R_\Theta^\top(\dot{v}^n - g^n), \tag{1d}$$

where the measurements in the North-East-Down (NED) frame (an Earth-fixed local reference frame assumed to be inertial) have superscript n, and measurements in the body-fixed frame have superscript b. For the purpose of stability analysis, the system is assumed to be deterministic such that noise is disregarded. This follows similar approaches as Fossen and Strand (1999) and Nguyen et al. (2007). The vector $p_m^n \in \mathbb{R}^2$ is the measured position in North and East. A vertical measurement may also be obtained through GNSS, but it is typically of low quality, and is not used here; see Section 3.2. The measured angle $\psi_m^n \in \mathbb{R}$ includes the low frequency yaw angle ψ and the wave-induced heading oscillations ψ_w, which are assumed to be small (Fossen and Strand, 1999). The angular velocity ω^b, which takes values in $\mathbb{R}^3$, is continuous and bounded, and the gyro bias is constant with a known bound $||b_g|| \leq M_b$. The vector $f_m^b \in \mathbb{R}^3$ is the measured specific force [2], including the acceleration of the vessel $\dot{v}^n$ and the acceleration due to gravity $g^n \in \mathbb{R}^3$. $R_\Theta \in \mathbb{R}^{3\times3}$ is the rotation matrix about the z, y, x-axes (Fossen, 2011, Ch. 2). We assume f_m^b is non-biased, bounded $||f_m^b|| \leq M_f$, and the derivative of the actual specific force $\dot{f}^b$ is continuous and bounded. Furthermore, there exists a constant $c_{obs} > 0$ such that $||c^b \times f_m^b|| > c_{obs}$, $c^b = [\cos(\psi_m^n), -\sin(\psi_m^n), 0]^\top$.

3 Candidate Observers and Controller

Two observers based on two philosophically different models of the same vessel are presented in the next sections. The relationship between the models are as follows:

$$\eta + \eta_w \equiv [p_{(1,1)}^n, p_{(2,1)}^n, \Theta_{(3,1)}]^\top \tag{2a}$$
$$\nu + \nu_w \equiv [v_{(1,1)}^b, v_{(2,1)}^b, \omega_{(3,1)}^b]^\top, \tag{2b}$$

with the subscript (i, j) denoting the elements of the corresponding vectors. On the left-hand side we have the position vector $\eta + \eta_w \in \mathbb{R}^3$ (North, East, yaw) and velocity vector $\nu + \nu_w \in \mathbb{R}^3$ (surge, sway, yaw) split into low-frequency and wave-frequency components. η and ν will later be estimated in the model-based observer and marked with a hat. On the right-hand side we have the low-frequency and wave-frequency position $p_{(1:2)}^n \in \mathbb{R}^2$ (North, East) and yaw $\Theta_{(3,1)}$, and velocity $v_{(1:2)}^b \in \mathbb{R}^2$ (surge, sway) and yaw $\omega_{(3,1)}^b$. Two consecutive elements of a vector are denoted with subscript $(1:2)$. p^n and $v^n := R_\Theta v^b$ are estimated in the signal-based observer and marked with a hat. Note that $\Theta_{(3,1)} \equiv \psi + \psi_w \approx \psi$.

3.1 Model-based observer

We have chosen to work with the nonlinear passive observer (Fossen and Strand, 1999) since it is an intuitive observer to tune, and it has global stability properties. This observer is based on the DP control plant model (Sørensen, 2011), which is a simplification of the real vessel dynamics. The inputs to the observer are the measurement $y = [p_m^{n\top}, \psi_m^n]^\top \in \mathbb{R}^3$ and the control input $\tau \in \mathbb{R}^3$. The 3 degree of freedom (DOF) model-based observer algorithm for a ship-shaped vessel in DP can be written as (Fossen and Strand, 1999)

$$\dot{\hat{\xi}} = A_\omega \hat{\xi} + K_{1,\omega}\tilde{y} \tag{3a}$$
$$\dot{\hat{\eta}} = R(\psi_m^n)\hat{\nu} + K_2\tilde{y} \tag{3b}$$
$$\dot{\hat{b}} = -T_b^{-1}\hat{b} + K_3\tilde{y} \tag{3c}$$
$$M\dot{\hat{\nu}} = -D_L\hat{\nu} + R^\top(\psi_m^n)\hat{b} + \tau + R^\top(\psi_m^n)K_4\tilde{y} \tag{3d}$$
$$\hat{y} = \hat{\eta} + W\hat{\xi}, \tag{3e}$$

where $\hat{\xi} \in \mathbb{R}^6, \hat{\eta}, \hat{\nu}, \hat{b} \in \mathbb{R}^3$ are the state estimates. The wave states $\xi \in \mathbb{R}^6$, low frequency position vector η and velocity vector ν, and the bias force vector $b \in \mathbb{R}^3$. $\tilde{y} := y - \hat{y}$ is the measurement estimation error, and $K_{1,\omega} \in \mathbb{R}^{6\times3}, K_2, K_3, K_4 \in \mathbb{R}^{3\times3}_{>0}$ are the observer gain-matrices. $A_\omega \in \mathbb{R}^{6\times6}$ is a Hurwitz matrix containing wave parameters, $R(\psi) \in \mathbb{R}^{3\times3}$ is the rotation matrix about the z-axis (Fossen, 2011, Ch. 2), $M = M^\top \in \mathbb{R}^{3\times3}$ is the inertia matrix including added mass, $D_L \in \mathbb{R}^{3\times3}$ is the linear damping coefficient matrix including second-order wave-induced damping, and $T_b \in \mathbb{R}^{3\times3}$ is a diagonal matrix of bias time constants. The first-order model (3c) accounts for *slowly-varying* environmental disturbances from mean wind, current, and second-order wave loads, as well as unmodeled vessel dynamics.

(A1) The bias force dynamics (3c) are assumed to account for only slowly-varying loads (Fossen and Strand, 1999).

This is a good assumption in steady state, but does not capture rapid variations in the bias force due to transients, e.g., heading changes or wave trains. Wave filtering is achieved by separating the wave-frequency motion estimate $\hat{\eta}_w = W\hat{\xi}$, $W = [0_{3\times3}, I_{3\times3}]$ from the low frequency estimate $\hat{\eta}$, giving the output from the model-based observer $\hat{\eta}_1 := \hat{\eta}$ and $\hat{\nu}_1 := \hat{\nu}$. The model-based

[2] Specific force is the physical acceleration experienced by an object, consisting of the acceleration of the object and the acceleration due to gravity, i.e., it is the *measurable* acceleration, with unit $[m/s^2]$.

estimation error dynamics, can be written compactly as

$$\dot{e}_1 = F_1(e_1), \tag{4}$$

with state vector

$$\begin{aligned} e_1 :=& x_1 - \hat{x}_1 \\ =& [(\xi - \hat{\xi})^\top, (b - \hat{b})^\top, (\eta - \hat{\eta})^\top, (\nu - \hat{\nu})^\top]^\top \in \mathbb{R}^{15}. \end{aligned}$$

Claim 1: Under Assumption (A1), the origin of the estimation error dynamics (4) is uniformly globally exponentially stable (UGES). □
Proof: See Fossen and Strand (1999). □

3.2 Signal-based observer

Grip et al. (2015) propose a nonlinear observer, for GNSS-aided inertial navigation with biased gyro measurements. It is based on the kinematic model (Fossen, 2011) with an angular and a translational part, relating the position, velocity, and acceleration of the vessel in 6 DOF. The inputs to the signal-based observer are p^n_m, ψ^n_m, ω^b_m, and f^b_m from (1). The rotation matrix R_Θ (about the z, y, x-axis) is estimated directly, giving

$$\dot{\hat{R}}_\Theta = \hat{R}_\Theta S(\omega^b_m - \hat{b}_g) + \sigma L_p \hat{J} \tag{5a}$$

$$\dot{\hat{b}}_g = \text{Proj}_{M_b}(\hat{b}_g, -L_I \text{vex}(\mathbb{P}_a(\hat{R}^\top_{\Theta s} L_P \hat{J}))), \tag{5b}$$

where $\hat{R}_\Theta$ is the rotation matrix estimate, $\hat{b}_g$ is the gyro bias estimate, and the angular rate estimate is $\hat{\omega}^b := \omega^b_m - \hat{b}_g$. The projection function $\text{Proj}_{M_b}(\cdot,\cdot)$ (Grip et al., 2015, Appendix) ensures that $||\hat{b}_g|| \leq M_{\hat{b}}$, and the $S(\cdot)$, $\text{vex}(\cdot)$, and $\mathbb{P}_a(\cdot)$ operators are defined in the footnote [3]. $\hat{R}_{\Theta s}$, appearing in (5b), is saturated elementwise with bound 1; $\hat{R}_{\Theta s} := \text{sat}_1(\hat{R}_\Theta)$. The gain-matrices are $L_P \in \mathbb{R}^{3\times3}_{>0}, L_I \in \mathbb{R}^{3\times3}_{>0}$, and $\sigma \geq 1$ is a scaling factor that is tuned to achieve stability. $\hat{J}$ is a stabilizing term (Grip et al., 2015, (3) and (5)) that takes ψ^n_m measured by the compass, and the specific force measurement f^b_m as input. The translational observer algorithm is

$$\dot{\hat{p}}_I = \hat{p}^n_{(3,1)} + k_{pipi}\tilde{p}_I \tag{6a}$$

$$\dot{\hat{p}}^n = \hat{v}^n + C_p e \tag{6b}$$

$$\dot{\hat{v}}^n = \hat{f}^n + g^n + C_v e \tag{6c}$$

$$\dot{\xi}_f = -\sigma L_p \hat{J} f^b_m + C_\xi e \tag{6d}$$

$$\hat{f}^n = \hat{R}_\Theta f^b_m + \xi_f, \tag{6e}$$

with estimates $\hat{p}_I, \hat{p}^n, \hat{v}^n$ and $\hat{f}^n$, $\hat{R}_\Theta$ is from (5), and ξ_f is a correction term on the specific force estimate. (6b-e) are standard kinematic observer equations, and (6a) is an addition from Bryne, Fossen, and Johansen (2015) that comes instead of using the vertical GNSS position measurement height, as mentioned in Section 2. The augmentation is motivated by the fact that a marine vessel in normal operation oscillates in heave about the mean sea surface. It may be assumed that:

(A2) The mean vertical position of the vessel over time is zero (Godhaven, 1998), $p_I = 0$.

p_I is called the *virtual vertical reference*. In (6a) the vertical position estimate $\hat{p}^n_{(3,1)}$ is integrated to give $\hat{p}_I$, which is compared with p_I and used as the driving error for the vertical dynamics. For more details, see Bryne et al. (2015). The driving error is $e := [\tilde{p}_I, \tilde{p}^\top]^\top \in \mathbb{R}^3$ with $\tilde{p} := p^n_m - \hat{p}^n_{(1:2)} \in \mathbb{R}^2$, $\tilde{p}_I := p_I - \hat{p}_I = 0 - \hat{p}_I \in \mathbb{R}$. The correction gain-matrices are

$$C_p = \begin{bmatrix} 0_{2\times1} & K_{pp} \\ k_{ppi} & 0_{1\times2} \end{bmatrix} \quad C_v = \begin{bmatrix} 0_{2\times1} & K_{vp} \\ k_{vpi} & 0_{1\times2} \end{bmatrix} \quad C_\xi = \begin{bmatrix} 0_{2\times1} & K_{\xi p} \\ k_{\xi pi} & 0_{1\times2} \end{bmatrix}.$$

The North and East gain components are $K_{pp}, K_{vp}, K_{\xi p} \in \mathbb{R}^{2\times2}_{>0}$, and the down gains are $k_{pipi}, k_{ppi}, k_{vpi}, k_{\xi pi} \in \mathbb{R}_{>0}$. The signal-based estimation error dynamics are written compactly as

$$\dot{e}_2 = F_2(e_2), \tag{7}$$

with state vector

$$\begin{aligned} e_2 :=& x_2 - \hat{x}_2 = [(r - \hat{r})^\top, (b_g - \hat{b}_g)^\top, (p_I - \hat{p}_I), \\ & (p^n - \hat{p}^n)^\top, (v^n - \hat{v}^n)^\top, (f^n - \hat{f}^n)^\top]^\top \in \mathbb{R}^{22}, \end{aligned}$$

with $r := [R_{\Theta(1,:)}, R_{\Theta(2,:)}, R_{\Theta(3,:)}]^\top \in \mathbb{R}^9$ and $\hat{r}$ defined accordingly. ':' denotes all elements of the row/column.
Claim 2: Under Assumption (A2), with inputs as described in (1), the origin of the signal-based estimation error dynamics (7) is UGES. □
Proof: See Grip et al. (2015) and Bryne et al. (2015). □
The output from the signal-based observer is written using (2), so that $\hat{\eta}_2 := [\hat{p}^n_{(1,1)}, \hat{p}^n_{(2,1)}, \hat{\Theta}_{(3,1)}]^\top$, $\hat{\nu}_2 := [\hat{v}^b_{(1,1)}, \hat{v}^b_{(2,1)}, \hat{\omega}^b_{(3,1)}]^\top$, where the heading angle estimate $\hat{\Theta}_{(3,1)}$ is extracted from $\hat{R}_\Theta$, and $\hat{v}^b = \hat{R}^\top_\Theta \hat{v}^n$. Because this observer relies on the specific force measurements instead of estimating the bias force, it reacts fast and accurately to transients. Here, no wave filter is included so $\hat{\eta}_2$ and $\hat{\nu}_2$ capture the combined low-frequency and wave-frequency motion. For shorter periods of time this may be acceptable, which is the case during transients.

3.3 Controller

The control objective is to control the vessel to the desired time-varying trajectory $\eta_d(t)$ with the desired ve-

[3] For a vector $x \in \mathbb{R}^3$, $S(x)$ denotes a skew-symmetric matrix so that for any $y \in \mathbb{R}^3$, $S(x)y = x \times y$, where $\times$ denotes the cross product. The skew-symmetric part of a matrix X is denoted by $\mathbb{P}_a = \frac{1}{2}(X - X^\top)$. The linear function $\text{vex}(X)$, with X skew symmetric is defined so that $S(\text{vex}(X)) = X$ and $\text{vex}(S(x)) = x$.

locity trajectory $\nu_d(t)$. The proposed control law is

$$\begin{aligned}\dot{\zeta}_s &= \hat{\eta}_s - \eta_d \\ \tau &= -K_p R^\top(\psi_m^n)(\hat{\eta}_s - \eta_d) - K_d(\hat{\nu}_s - \nu_d) \\ &\quad - K_i R^\top(\psi_m^n)\zeta_s + M\dot{\nu}_d + D_L\nu_d.\end{aligned} \tag{8}$$

$\tau \in \mathbb{R}^3$ is the commanded thrust vector, $K_p, K_d, K_i \in \mathbb{R}^{3\times3}_{\geq 0}$ are gain-matrices, and $\hat{\eta}_s$ and $\hat{\nu}_s$ are the estimates from the model-based observer when $s = 1$, and from the signal-based observer when $s = 2$. ζ_s compensates for the unknown bias force vector b with dynamics $\dot{b} = -T_b^{-1}b$. The last two terms in (8) are feedforward terms of the desired acceleration and desired velocity. For the stability analysis of the controller, it is assumed that:

(A3) The yaw rate $\omega^b_{(3,1)}$ (also denoted $\nu_{(3,1)}$) is bounded, $|\omega^b_{(3,1)}| < r_{max}$, and K_i and T_b commute with $R(\psi)$ [4] (Lindegaard and Fossen, 2003).

The following result is proven in Lindegaard and Fossen (2003).

Claim 3: If Assumption (A3) holds, and the controller gains are chosen so that the system matrix A_c (see below) is Hurwitz, the origin of the tracking error dynamics, consisting of the control plant model using control input with *state feedback*, (8) inserted the real states η, ν, is UGES. □

We note, for later use, that the tracking error dynamics have the form $\dot{e}_0 = T^\top(\psi)A_cT(\psi)e_0$ with

$$\begin{aligned}e_0 &= [\xi^\top, b^\top, (\eta-\eta_d)^\top, (\nu-\nu_d)^\top, \zeta^\top] \\ A_c &= \begin{bmatrix} A_\omega & 0 & 0 & 0 & 0 \\ 0 & -T_b^{-1} & 0 & 0 & 0 \\ 0 & 0 & 0 & I & 0 \\ 0 & I & -M^{-1}K_p & -M^{-1}(D_L+K_d) & -M^{-}K_i \\ 0 & 0 & I & 0 & 0 \end{bmatrix}, \\ T(\psi) &= \text{blkdiag}([I, R^\top(\psi), R^\top(\psi), I, R^\top(\psi)]),\end{aligned}$$

where $T(\psi)$ is a block diagonal matrix. A Lyapunov function of the form $V_0(e_0, \psi) := e_0^\top T^\top(\psi)PT(\psi)e_0$ with $P = P^\top > 0$, where P satisfies the linear matrix inequality (LMI) $PA_c + A_c^\top P < 0$, that verifies the UGES property asserted in Claim 3.

4 Hybrid system

In this paper we propose a new hybrid strategy for DP systems in order to cope with both stationary and transient dynamics. In general, a hybrid system $\mathcal{H} = (C, F, D, G)$ is written formally as

$$x \in C \;\; \dot{x} \in F(x) \tag{9a}$$
$$x \in D \;\; x^+ \in G(x), \tag{9b}$$

where x is the hybrid state, C is the flow set, F is the flow map, D is the jump set, and G is the jump map. When x is in C, then the states are allowed to flow, and when x is in D the states are allowed to jump (Goebel et al., 2012). In this section the hybrid DP control system is assembled, starting with the performance monitoring and switching logic that choose the appropriate estimates to use in output feedback with (8). The performance monitoring and switching logic dynamics can be written as:

$$\dot{m}_i = 0, \qquad i = \{1, ..., n\} \tag{10a}$$
$$\dot{t}_m = -1 \tag{10b}$$
$$\dot{s} = 0 \tag{10c}$$
$$m_i^+ = \begin{cases} ||\hat{\eta}_{1(1:2)} - \hat{\eta}_{2(1:2)}||, & \text{for } i = 1 \\ m_{i-1}, & \text{for } i = \{2, ..., n\} \end{cases} \tag{10d}$$
$$t_m^+ = T \tag{10e}$$
$$s^+ = \begin{cases} 1, & \text{if } \bar{m} \leq \epsilon_{ss} \\ 2, & \text{if } \bar{m} \geq \epsilon_{tr} \\ 2, & \text{if } \nu_{d(3,1)} \geq \delta \\ s, & \text{otherwise,} \end{cases} \tag{10f}$$

where m_i are monitoring states, t_m is a timer, and s is the switching signal. In order to evaluate the performance of the observers, we choose to compute the difference in estimation error in North and East $(p_m^n - \hat{\eta}_{2(1:2)}) - (p_m^n - \hat{\eta}_{1(1:2)}) = (\hat{\eta}_{1(1:2)} - \hat{\eta}_{2(1:2)})$, and take the Euclidean norm of this difference, see (10d). This signal may oscillate a lot, so we take the average of n of the past values that are saved in the shift register of size n with state $m \in \mathbb{R}^n$, i.e., $\bar{m} = \frac{1}{n}\sum_{i=1}^n m_i$. We call $\bar{m}$ the performance monitoring signal, and switch based upon this quantity in (10f). m does not change during flows, (10a). During flows, t_m decreases with unitary rate (10b), and is reset to T during jumps. A new jump is triggered when a new position measurement is available, when $t_m = 0$, so the position measurement has sample time T. The jump map for the switching signal s, including performance and heading change monitoring is (10f), where $\epsilon_{ss} \geq 0$ is the estimation difference we expect to see in steady state, and $\epsilon_{tr} \geq 0$ is the estimation difference we expect to see during a transient. Choose $\epsilon_{tr} > \epsilon_{ss}$ with some margin to provide hysteresis that suppresses unnecessary switching back and forth. The signal-based observer is chosen in closed loop if the desired yaw rate $\nu_{d(3,1)}$ is larger than a threshold $\delta \geq 0$, as we know that the forces on the vessel hull will change rapidly in this situation. s does not change during flows (10c).

For later use, we look closer at the steady state behavior of the performance monitoring states. Inserting for the

[4] $K_i = \text{diag}([k_1, k_1, k_2]), T_b = \text{diag}([t_1, t_1, t_2])$ are used. The North and East gains/time constants are equal, which for a marine vessel is justified, since the environmental changes have roughly the same dominating frequencies in surge and sway.

steady-state observer estimates we have that $\hat{\eta}_{1(1:2)} = \eta_{(1:2)}$ (Claim 1), and $\hat{\eta}_{2(1:2)} = p^n_{(1:2)}$ (Claim 2). During steady state, the performance monitoring states m_i, $i = \{1, ..., n\}$, are

$$m_i = \left(||\eta_{(1:2)} - p^n_{(1:2)}||\right)_{i-1} = \left(||\eta_{w(1:2)}||\right)_{i-1}, \quad (11)$$

corresponding to the norm of the wave-frequency motion $\eta_w = W\xi$ in North and East, for each sample i in the shift register. The wave states ξ go to zero during steady state, since A_ω in (3a) is Hurwitz. In this case $\bar{m}$ is also zero, and we would like to use the model-based observer estimates in output feedback with (8) during steady state. This is because these estimates are wave filtered, and hence reduce the wear and tear on the propulsion system. During a transient, the observers do not agree, and then $\bar{m}$ is larger. Since the signal-based observer presumably performs better in transients, these estimates are used in closed loop during these times.

The control plant model and the kinematic model represent, with some overlap, the same underlying dynamics being the motion of the vessel. We assume that:

(A4) The solutions to the control plant model and kinematic model dynamics are forward complete [5].

Then the solutions exist for all positive time. The tracking error analysis in Lindegaard and Fossen (2003) (Claim 3) makes sure that x_1 behaves as it is meant to, i.e., η converges to η_d and ν converges to ν_d. From the relation between the control plant model and kinematic model (2), we have that $[p^{n\top}_{(1:2)}, \Theta_{(3,1)}]^\top$ goes to η_d, and $[v^{b\top}_{(1:2)}, \omega^b_{(3,1)}]^\top$, goes to ν_d. The heave, roll, and pitch states in the kinematic model are not controlled, and hence do not converge to a reference. Therefore the kinematic model with state x_2 is not included in the hybrid analysis. We define the state vector of the hybrid system as

$$\begin{aligned} x &:= (x_1, \zeta_s, \hat{x}_1, \hat{x}_2, m, t_m, s) \quad (12)\\ &\in \mathbb{R}^{15} \times \mathbb{R}^3 \times \mathbb{R}^{15} \times \mathbb{R}^{22} \times \mathbb{R}^n \times [0, T] \times \{1, 2\}, \end{aligned}$$

consisting of the control plant model state x_1, the integral state in the control law ζ_s, the model-based observer estimates $\hat{x}_1$, the signal-based observer estimates $\hat{x}_2$, the performance monitoring states m, the timer t_m, and the switching signal s. The flow dynamics of the hybrid system constitutes the vessel described by the control plant model, controller, observer, and timer dynamics. The states $x_1, \zeta_s, \hat{x}_1$, and $\hat{x}_2$ do not change during jumps, i.e., $x_1^+ = x_1,\ \zeta_s^+ = \zeta_s$, and so on. The dynamics for $m,\ t_m$, and s are given by (10). Flows are allowed when $x \in C$, and jumps are allowed when $x \in D$, defined by

$$C := \mathbb{R}^{55+n} \times [0, T] \times \{1, 2\} \quad (13)$$
$$D := \mathbb{R}^{55+n} \times \{0\} \times \{1, 2\}. \quad (14)$$

[5] A solution with an unbounded time domain is called complete, (Goebel et al., 2009, p. 41).

5 Stability

We are analyzing stability of the set

$$\begin{aligned} \mathcal{A} := C \cap\ &(\{x_{1d}\} \times \{0\} \times \{x_{1d}\} \\ &\times \{x_2\} \times \{0\} \times [0, T] \times \{1, 2\}). \end{aligned} \quad (15)$$

This corresponds to the vessel tracking the desired trajectory, with $x_{1d} = [0, 0, \eta_d^\top, \nu_d^\top]^\top$, and the controller integral state ζ_s converging to zero. The model-based estimates being equal to the control plant model state x_1, which goes to x_{1d}, and the signal-based estimates being equal to the kinematic model state x_2. The performance monitoring states m go to zero, as discussed around (11), and the timer t_m and the switching signal s stay within $\mathcal{A}$ by design.

Theorem 1 *Under Assumptions (A1-A4) the set $\mathcal{A}$ given by* (15) *is GAS for the hybrid system given by the control plant model, the observers* (3), (5)-(6)*, the controller* (8)*, the performance monitoring and switching logic* (10)*, and the flow and jump sets* (13)-(14). □

Proof: The proof follows from Goebel et al. (2009), Corollary 19. By splitting the control law (8) into a state feedback part and a part that is due to estimation error, the tracking error dynamics and observer error dynamics can be written in a cascaded structure,

$$\dot{e}_0 = F_0(e_0) + g(e_0, e_s) \quad (16a)$$
$$\dot{e}_1 = F_1(e_1) \quad (16b)$$
$$\dot{e}_2 = F_2(e_2) \quad (16c)$$
$$e_0^+ = e_0,\ e_1^+ = e_1,\ e_2^+ = e_2. \quad (16d)$$

(16a) is the tracking error dynamics with tracking error $e_0 = [\xi^\top, b^\top, (\eta - \eta_d)^\top, (\nu - \nu_d)^\top, \zeta^\top]^\top$ and estimation errors e_s, with $s = 1$ model-based estimation error, and $s = 2$ signal-based estimation error. $g(e_0, e_s)$ is the additional control input due to estimation error, where $g(e_0, e_s) = K_p R^\top(\psi^n_m)(\eta - \hat{\eta}_s) + K_d(\nu - \hat{\nu}_s) + K_i R^\top(\psi^n_m)(\zeta - \zeta_s)$. The switching signal s decides which observer perturbs the tracking error dynamics. (16b,c) are the model-based and signal-based estimation error dynamics. The rest of the observer error dynamics are given by (10). The flow and jump sets for (10) and (16) are:

$$C' := \mathbb{R}^{55+n} \times [0, T] \times \{1, 2\} \quad (17)$$
$$D' := \mathbb{R}^{55+n} \times \{0\} \times \{1, 2\} \quad (18)$$

To prove Theorem 1, it is sufficient to prove global asymptotic stability (GAS) of the set

$$\mathcal{A}' := \{0_{55+n}\} \times [0, T] \times \{1, 2\}, \tag{19}$$

for the hybrid system $\mathcal{H} := (C', F, D', G)$ given by (10) and (16)-(18). This is done in two steps.

Step 1. We prove GAS of $\mathcal{A}'$ for $\mathcal{H}_\beta := (C_\beta, F, D_\beta, G)$, which is $\mathcal{H}$ with the flow and jump sets intersected with $\beta\mathbb{B} \times \mathbb{R}^{37+n}$ for $\beta > 0$ and unit ball $\mathbb{B} \in \mathbb{R}^{18}$; $C_\beta := C' \cap (\beta\mathbb{B} \times \mathbb{R}^{37+n})$ and $D_\beta := D' \cap (\beta\mathbb{B} \times \mathbb{R}^{37+n})$. Firstly, the compact set

$$\mathcal{A}_1 := \{\beta\mathbb{B}\} \times \{0_{37+n}\} \times [0, T] \times \{1, 2\}, \tag{20}$$

is GAS for $\mathcal{H}_\beta$. This follows from the analysis in Fossen and Strand (1999), Bryne et al. (2015) and Grip et al. (2015) resulting in UGES origin of the observer error dynamics (Claim 1 and 2). Then, we prove GAS of $\mathcal{A}'$ for $\mathcal{H}|_{\mathcal{A}_1} := (C' \cap \mathcal{A}_1, F, D' \cap \mathcal{A}_1, G)$. When the solution is in $\mathcal{A}_1$, we have state feedback so that (16a) is $\dot{e}_0 = F_0(e_0)$, since $e_s = 0$, and $g(e_0, 0) = 0$. The analysis in Lindegaard and Fossen (2003) give UGES origin of the tracking error dynamics with state feedback (Claim 3). Applying Corollary 19 in Goebel et al. (2009), we have that the compact set $\mathcal{A}_1$ is GAS for $\mathcal{H}_\beta$, and that the compact set $\mathcal{A}' \subset \mathcal{A}_1$ is GAS for $\mathcal{H}|_{\mathcal{A}_1}$. Then $\mathcal{A}'$ is GAS for $\mathcal{H}_\beta$.

Step 2. We use this preliminary result to prove GAS of $\mathcal{A}'$ for $\mathcal{H}$ without restrictions on e_0 in the flow and jump sets. The solutions of $\mathcal{H}$ are the solutions of $\mathcal{H}_\beta$ when $e_0 \in \beta\mathbb{B}$. The only thing left to prove is that the basin of attraction is the entire space, so that for each solution, β can be chosen large enough so that the $\beta\mathbb{B}$ intersection has no effect. The observer solutions e_s can be bounded by $||e_s(t)|| \leq \lambda_1 ||e_s(t_0)|| e^{-\lambda_2(t-t_0)}$ for $\lambda_1, \lambda_2 > 0$ that are dependent on initial condition $e_s(t_0)$. Integrating $e_s(t)$ over time, we get

$$\int_{t_0}^{\infty} ||e_s(t, t_0, e_s(0))|| dt \leq \phi(||e_s(t_0)||), \quad \forall t_0 \geq 0,$$

with $\phi(||e_s(t_0)||) = \frac{\lambda_1}{\lambda_2}||e_s(t_0)||$. $g(e_0, e_s)$ can be bounded in terms of e_s by $||g(e_0, e_s)|| \leq \gamma ||e_s||$, $\gamma \geq ||[K_p,\ K_d,\ K_i]^\top||$. Then, the only state that can grow unbounded is e_0, but this is ruled out by the following. The Lyapunov function $V_0(e_0, \psi)$, defined below Claim 3, for (16a) with $g(e_0, e_s) = 0$ and $F_0(e_0) = T^\top(\psi) A_c T(\psi) e_0$ satisfies

$$\left|\left| \frac{\partial V_0(e_0, \psi)}{\partial e_0} \right|\right| ||e_0|| \leq c_1 ||e_0||^2, \quad \forall ||e_0|| \geq \mu \tag{21a}$$

$$\left|\left| \frac{\partial V_0(e_0, \psi)}{\partial e_0} \right|\right| \leq c_2, \quad \forall ||e_0|| \leq \mu \tag{21b}$$

with $c_1 = 2\lambda_{max}(P)$ and $c_2 = 2\lambda_{max}(P)\mu$, with $\lambda_{max}(P)$ being the largest eigenvalue of P. (21b) holds for all headings ψ. (21) ensures that e_0 stays bounded (Loria, Fossen, and Panteley, 2000), so that each solution of $\mathcal{H}$ has to converge to $\mathcal{A}'$ because it is a solution to the system $\mathcal{H}_\beta$ for large enough β and the solutions of $\mathcal{H}_\beta$ converge. Hence, $\mathcal{A}'$ in (19) is GAS for the hybrid system $\mathcal{H}$ given by (10) and(16)-(18), which concludes the proof. □

When applying Assumption (A1) we assume that the control plant model is an exact deterministic model of the real vessel dynamics. Then there may only be switching due to reference changes and due to transients during initialization. However, as shown through experiments in Section 6, switching based on performance is triggered because Assumption (A1) of slowly-varying bias loads does not hold during transients. Performing an analysis of the hybrid system with randomness is a topic for further work, see Teel et al. (2014).

6 Experimental setup, results and discussion

The model-scale experiments were conducted with C/S Inocean Cat I Drillship, a 1:90 scale model with dimensions (length, beam) = (2.578 m, 0.44 m) in the Marine Cybernetics Laboratory (MCLab) at NTNU. The full-scale DP data was collected during the AMOS DP Research Cruise 2016 (ADPRC'16) onboard R/V Gunnerus, see Skjetne et al. (2017) for details. The model-based observer was in both cases tuned using tuning rules in Fossen (2011), Ch. 11, for good steady state, and adequate transient performance. The same IMUs were used to provide input to the signal-based observer both in model-scale and full-scale, showing that the proposed hybrid observer setup is robust to large variations in signal-to-noise ratio. In full-scale, the signal-based observer tuning from Bryne et al. (2015) was tweaked to work better for R/V Gunnerus, but in the MCLab the tuning was found from scratch. Tuning of the controller in the MCLab was found using standard PID tuning rules (Fossen, 2011, Ch. 12), which were tweaked to work well with both observer estimates in feedback. The algorithms were coded in Matlab/Simulink and run in NI Veristand [6] software.

6.1 Model-scale experiments

Wind loads constitute a lot of the mean forces on the vessel hull, and since wind is not available in the MCLab, the directional dependence of the bias force that is seen in full-scale applications was less prominent in the lab. Hence, switching based on observer performance was triggered by pushing the model off setpoint using a boathook, inducing an unknown, rapid transient, see Figure 2. The model is pushed off setpoint twice; at time

[6] The Bogacki-Shampine solver (Matlab ode23) was used with fixed step 0.01 s, www.ni.com/veristand/.

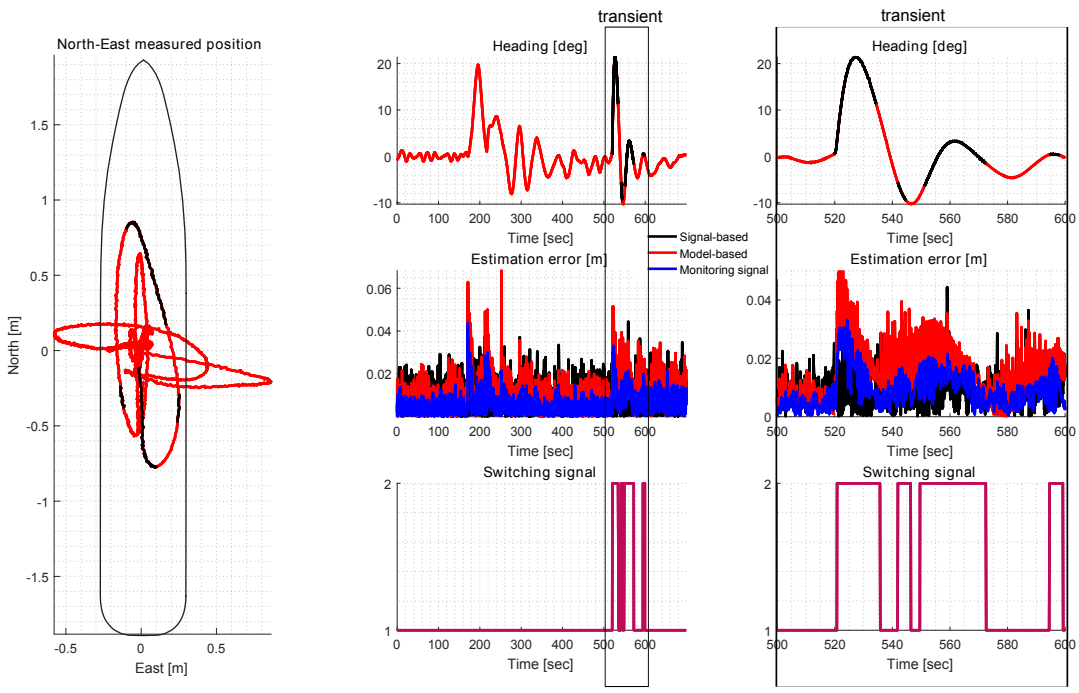

Fig. 2. Closed-loop control: C/S Inocean Cat I Drillship is pushed off position using a boat-hook at time 170 s and 520 s. North-East position track (left), heading, estimation error, monitoring signal and switching signal (middle), details of the second transient (right). Position and heading trajectories are red when model-based estimates are used in closed loop, and black for signal-based estimates. Environmental conditions corresponding to rough full-scale sea state with significant wave height $H_s = 3.6$ m, peak period $T_p = 10.4$ s, head sea, no wind nor current, $\epsilon_{tr} = 0.02, \epsilon_{ss} = 0.005, \delta = 0.05$.

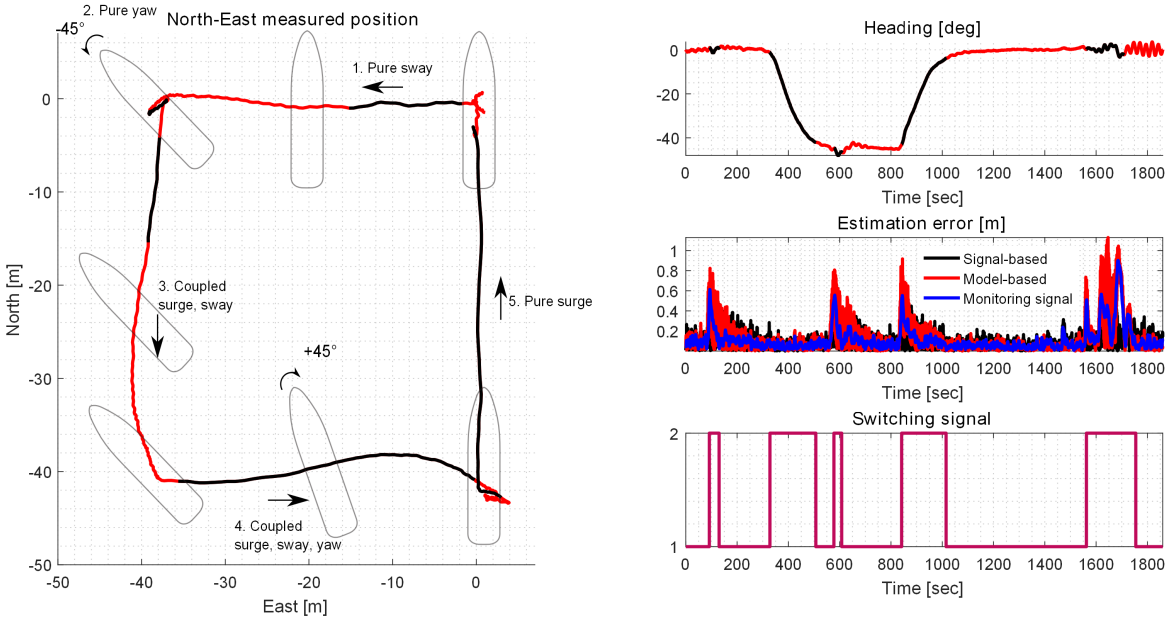

Fig. 3. Estimation: R/V Gunnerus is doing a DP 4 corner maneuver, staring at (0,0) and moving as indicated by the arrows. North-East position track (left), heading, observer estimation error and monitoring signal, and switching signal (right). The position and heading trajectories are red when the model-based estimates should be used in closed loop, and black when the signal-based estimates should be used in closed loop. Environmental conditions: current 0.3 m/s, 290°, wind 7 m/s, 260°, and waves with significant wave height $H_s = 0.2$ m, peak period $T_p = 13.6$ s, and direction 260°. $\epsilon_{tr} = 0.5, \epsilon_{ss} = 0.03, \delta = 0.2$.

170 s and 520 s. In the first transient, the observer is fixed with the model-based observer in closed loop. The vessel spends a long time coming back to the setpoint, since the estimates from the model-based observer (especially the velocity estimate) is off during the transient. In the second transient the observer is allowed to switch based on performance, and chooses the signal-based observer in closed loop for most of the transient, although there is some switching back and forth. The heading reaches steady state somewhat faster when the signal-based observer is in closed loop, *although comparison of the two pushes can be seen only as indications of performance since the conditions were not identical.* Brodtkorb et al. (2016) and the section below compares the model-based observer, signal-based observer and hybrid approach in closed loop and estimation performance on full-scale data, respectively. Switching during heading changes, based on desired yaw rate, worked well in the MCLab. How large δ is chosen should be dependent on the vessel size and the maximum desired yaw rate. The thrust usage when the model-based or the signal-based observer estimates were used in closed loop was not significantly different, though the signal-based estimates made the thrust more oscillatory, as expected.

6.2 Estimation based on full-scale measurements

Figure 3 shows estimation results on full-scale R/V Gunnerus data from a DP 4 corner maneuver, and that the hybrid observer switches due to transients. If the third and fourth parts of the maneuver were to be done close to other offshore infrastructure, R/V Gunnerus may have been required to either reduce the speed, or choose another control strategy in order to stay on the desired straight-line segments of the square. In the fifth maneuver, a pure surge motion should not induce much transients, however in this dataset the heading oscillates $\pm 3°$, and therefore the signal-based observer is chosen for most of the leg. Depending on the vessel size, propulsion system, and instrumentation, a smarter choice of controller could make the vessel stay on the desired path with a higher speed, reducing the vessel operation time.

Figure 4 and Table 1 show the cumulative estimation errors over time when the model-based, signal-based and hybrid observer (switching between the model-based and signal-based) are used for estimation on full-scale data. The hybrid observer has the lowest estimation error at the end of the time series in surge and sway, a bit lower than the signal-based observer, and much lower than the model-based observer, which accumulates estimation error fast during transients. The signal-based observer has the smallest estimation error in yaw; 34% lower than the model-based observer, and 28% lower than the hybrid observer. A reason may be that the signal-based observer uses more information about the yaw angle through the yaw rate to construct the estimate. Keep in mind that the maneuver R/V Gunnerus performs in this case includes a lot of transients, and therefore favors the signal-based observer over the model-based observer. In the case where there are more periods of steady state, the model-based observer and hybrid approach are more beneficial.

Table 1
Cumulative estimation errors for the model-based, signal-based and hybrid observers at the end of R/V Gunnerus' DP 4 corner maneuver.

Observer	Surge [m]	Sway [m]	Yaw [deg]
Model-based	1368.3	998.0	1372.7
Signal-based	964.3	949.9	902.9
Hybrid	945.1	901.3	1247.3

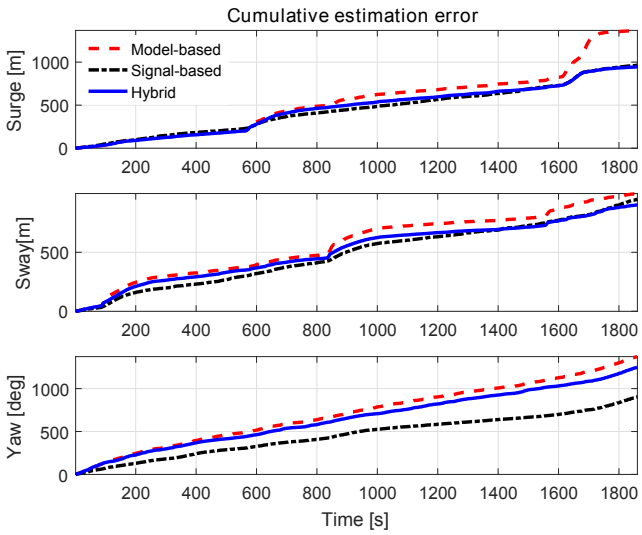

Fig. 4. Cumulative estimation error when the model-based, signal-based and hybrid observers are used for estimation on full scale field data from R/V Gunnerus doing a DP 4-corner maneuver.

7 Conclusion

A general hybrid control strategy for marine control systems providing a redundant design methodology for robustness to system errors was proposed in this paper. An example of a such control system improving the transient vessel response in dynamic positioning was given. Performance was shown through model-scale experiments, and estimation on full-scale field data.

Acknowledgements

Thanks to Vincenzo Calabrò and the rest of the Kongsberg Maritime team, Øivind Kjerstad, Mikkel E. N. Sørensen and Martin Heyn for collaboration during ADPRC'16, and to Torgeir Wahl for assistance in the MCLab.

References

Blanke, M., Kinnaert, M., Lunze, J., and Staroswiecki, M. (2003). *Diagnosis and Fault-tolerant Control*. Springer.

Brodtkorb, A.H., Værnø, S.A., Teel, A.R., Sørensen, A.J., and Skjetne, R. (2016). Hybrid observer for improved transient performance of a marine vessel in dynamic positioning. *NOLCOS, USA*.

Bryne, T.H., Fossen, T.I., and Johansen, T.A. (2015). A virtual vertical reference concept for GNSS/INS applications at the sea surface. *MCMC, Denmark*.

DNV-GL (2014). *DNV Rules for Classification of Ships, Part 6, Ch. 6.* DNV-GL service documents.

Fossen, T.I. (2011). *Handbook of Marine Craft Hydrodyamics and Motion Control*. Wiley.

Fossen, T.I. and Strand, J.P. (1999). Passive nonlinear observer design for ships using lyapunov methods: Full-scale experiments with a supply vessel. *Automatica*, 35(1), 3 – 16.

Girard, A.R., Howell, A.S., and Hedrick, J.K. (2005). Hybrid supervisory control for real-time embedded bus rapid transit applications. *IEEE Transactions on Vehicular Technology*, 54(5), 1684–1696. doi: 10.1109/TVT.2005.853466.

Godhaven, J.M. (1998). Adaptive tuning of heave filter in motion sensor. In *OCEANS '98 Conference Proceedings*, volume 1, 174–178 vol.1. doi: 10.1109/OCEANS.1998.725731.

Goebel, R., Sanfelice, R., and Teel, A.R. (2009). Hybrid dynamical systems robust stability and control for systems that combine continuous-time and discrete-time dynamics. *IEEE Control Systems Magazine, April 2009*, 28–93.

Goebel, R., Sanfelice, R.G., and Teel, A.R. (2012). *Hybrid Dynamical Systems, Modelling, Stability and Robustness*. Princeton University Press.

Grip, H.F., Fossen, T.I., Johansen, T.A., and Saberi, A. (2015). Globally exponentially stable attitude and gyro bias estimation with application to GNSS/INS integration. *Automatica*, 158–166.

Hassani, V., Sørensen, A.J., Pascoal, A.M., and Athans, M. (2017). Robust dynamic positioning of offshore vessels using mixed- synthesis modeling, design, and practice. *Ocean Engineering*, 129, 389 – 400.

Hassani, V., Sørensen, A.J., Pascoal, A.M., and Dong, N.T. (2012). Multiple model adaptive dynamic positioning. *9th {IFAC} Conference on Manoeuvring and Control of Marine Craft*, 45(27), 55 – 60.

Hespanha, J.P., Liberzon, D., and Morse, A.S. (2003). Hysteresis-based switching algorithms for supervisory control of uncertain systems. *Automatica*, 39(2), 263–272.

Hespanha, J.P. and Morse, A.S. (2002). Switching between stabilizing controllers. *Automatica*, 38(11), 1905–1917.

Hu, J., Prandini, M., and Sastry, S. (2005). Aircraft conflict prediction in the presence of a spatially correlated wind field. *IEEE Transactions on Intelligent Transportation Systems*, 6(3), 326–340. doi: 10.1109/TITS.2005.853699.

Kapinski, J., Deshmukh, J.V., Jin, X., Ito, H., and Butts, K. (2016). Simulation-based approaches for verification of embedded control systems: An overview of traditional and advanced modeling, testing, and verification techniques. *IEEE Control Systems*, 36(6), 45–64. doi:10.1109/MCS.2016.2602089.

Lindegaard, K.P. and Fossen, T.I. (2003). Fuel-efficient rudder and propeller control allocation for marine craft: experiments with a model ship. *IEEE Transactions on Control Systems Technology*, 11(6), 850–862.

Loria, A., Fossen, T.I., and Panteley, E. (2000). A separation principle for dynamic positioning of ships: Theoretical and experimental results. *IEEE TCST*, 8(2), 332–343.

Malladi, B.P., Sanfelice, R.G., Butcher, E., and Wang, J. (2016). Robust hybrid supervisory control for rendezvous and docking of a spacecraft. In *2016 IEEE 55th Conference on Decision and Control (CDC)*, 3325–3330. doi:10.1109/CDC.2016.7798769.

Miyazaki, M.R., Sørensen, A.J., and Vartdal, B.J. (2016). Reduction of fuel consumption on hybrid marine power plants by strategic loading with energy storage devices. *IEEE Power and Energy Technology Systems Journal*, 3(4), 207–217.

Nguyen, T.D., Sørensen, A.J., and Quek, S.T. (2007). Design of hybrid controller for dynamic positioning from calm to extreme sea conditions. *Automatica*, 43(5), 768–785.

Perez, T., Sørensen, A., and Blanke, M. (2006). Marine vessel models in changing operational conditionsa tutorial. *14th IFAC Symposium on Identification and System Parameter Estimation, IFAC Proceedings Volumes*, 39(1), 309 – 314. doi:http://dx.doi.org/10.3182/20060329-3-AU-2901.00044.

Sastry, S., Meyer, G., Tomlin, C., Lygeros, J., Godbole, D., and Pappas, G. (1995). Hybrid control in air traffic management systems. In *Proceedings of 1995 34th IEEE Conference on Decision and Control*, volume 2, 1478–1483 vol.2.

Skjetne, R., Kjerstad, Ø.K., Værnø, S.A.T., Brodtkorb, A.H., Sørensen, A.J., Sørensen, M.E.N., Breivik, M., Calabrò, V., and Vinje, B.O. (2017). AMOS DP research campain. *OMAE, Norway*.

Smogeli, Ø., Vik, B., Haugen, O., and Pivano, L. (2014). Risk management for control system software for the maritime and offshore oil and gas industries. *Proceedings of the IMCA Annual Seminar, London*.

Sørensen, A.J. (2011). A survey of dynamic positioning control systems. *Annual Reviews in Control*, 35(1), 123–136.

Teel, A.R., Subbaraman, A., and Sferlazza, A. (2014). Stability analysis for stochastic hybrid systems: A survey. *Automatica*, 50(10), 2435 – 2456.